Atmos. Chem. Phys. Discuss., https://doi.org/10.5194/acp-2017-447
Manuscript under review for journal Atmos. Chem. Phys.
Discussion started: 5 July 2017

Atmospheric Chemistry and Physics Discussions

Seasonal variation of fine- and coarse-mode nitrates and related aerosols over East Asia: Synergetic observations and chemical transport model analysis

Itsushi Uno[1], Kazuo Osada[2], Keiya Yumimoto[1], Zhe Wang[1,3], Syuichi Itahashi[4], Xiaole Pan[3], Yukari Hara[1], Yugo Kanaya[5], Shigekazu Yamamoto[6], Thomas Duncan Fiarlie[7]

[1] Research Institute for Applied Mechanics, Kyushu University, Kasuga Park 6-1, Fukuoka 816-8580, Japan
[2] Nagoya University, Graduate School of Environ. Studies, Furo-cho, Chikusa-ku, Nagoya, 464-8601, Japan
[3] Institute of Atmospheric Physics, CAS, Beijing, China
[4] Central Research Institute of Electric Power Industry, Abiko, Chiba, 270-1194, Japan
[5] Japan Agency for Marine-Earth Science and Technology, 3173-25 Showa-machi, Kanazawa-ku, Yokohama, 236-0001, Japan
[6] Fukuoka Institute of Health and Environmental Sciences, Mukaizano 39, Dazaifu, Fukuoka 818-0135, Japan
[7] NASA, Langley Research Center, Hampton, VA 23681-0001, U.S.A.

Correspondence to: Itsushi Uno (uno@riam.kyushu-u.ac)

Abstract. We analyzed long-term fine- and coarse-mode nitrate and related aerosols (SO_4^{2-}, NO_3^-, NH_4^+, Na^+, Ca^{2+}) synergetic observations at Fukuoka (33.52°N, 130.47°E) from August 2014 to October 2015. A Goddard Earth Observing System chemical transport model (GEOS-Chem) including dust and sea-salt acid uptake processes was used to assess the observed seasonal variation, and the impact of long-range transport (LRT) from the Asian continent. For fine aerosols (fSO_4^{2-}, fNO_3^-, and fNH_4^+), numerical results explained the seasonal changes, and a sensitivity analysis excluding Japanese domestic emissions clarified the LRT fraction at Fukuoka (85% for fSO_4^{2-}, 47% for fNO_3^-, 73% for fNH_4^+). Observational data for HNO_3, fNO_3^-, and coarse NO_3^- (cNO_3^-) confirmed that cNO_3^- made up the largest proportion of total nitrate (defined as the sum of fNO_3^-, cNO_3^- and HNO_3), constituting 40−55% of total nitrate during the winter, while HNO_3 gas constituted approximately 40% of total nitrate in summer, and fNO_3^- peaked during the winter. A numerical model reproduced the seasonal variations in fNO_3^-. For cNO_3^-, large-scale dust-nitrate outflow from China to Fukuoka was confirmed during all dust events that occurred between January and June. Modeled cNO_3^- was in good agreement with observations between July and November (mainly coming from sea salt-NO_3^-). However during the winter, the model underestimated cNO_3^- levels compared to the observed levels. The reason for this underestimation was examined statistically using multiple regression analysis (MRA). We used cNa^+, nss-cCa^{2+}, and cNH_4^+ as independent variables to describe the observed cNO_3^- levels; these variables were considered representative of sea salt-cNO_3^-, dust-cNO_3^-, and cNO_3^- accompanied by cNH_4^+ (cNH_4^+ term), respectively. The MRA results explained the observed seasonal changes in dust-cNO_3^- and indicated that the dust-acid uptake scheme reproduced the observed dust-nitrate levels even in winter. The annual average contributions of each component were 43% (sea salt-cNO_3^-), 19% (dust cNO_3^-), and 38% (cNH_4^+ term). The MRA dust-cNO_3^- component had a

Atmos. Chem. Phys. Discuss., https://doi.org/10.5194/acp-2017-447
Manuscript under review for journal Atmos. Chem. Phys.
Discussion started: 5 July 2017

Atmospheric Chemistry and Physics Discussions

high value during the dust season, and the sea salt component made a large contribution throughout the year. During the winter, cNH_4^+ term made a large contribution. The model did not include aerosol microphysical processes (such as condensation and coagulation between the fine anthropogenic aerosols NO_3^- and SO_4^{2-} and coarse particles), and our results suggest that inclusion of aerosol microphysical processes is critical when studying observed cNO_3^- formation, especially in winter.

1 Introduction

Long-range trans-boundary transport of dust and pollutants in East Asia, and their complex interactions, are an important environmental issue due to the recent rapid economic developments and changes in these areas (e.g., Lawrence and Lelieveld, 2010, Li *et al.* 2017, Zhang *et al*., 2017). Because of the heavy air pollution occurring in China, a great deal of research focuses mainly on fine-mode aerosols (i.e., $PM_{2.5}$, particle aerodynamic diameter < 2.5 μm). NOx emissions have been increasing rapidly over the past decade (e.g., Richter *et al*., 2002, Irie *et al*. 2016), and long-range nitrate transport is becoming increasingly important for regional nitrogen budget studies (e.g., Oita *et al*., 2016, Itahashi *et al*., 2016, 2017; Uno *et al*., 2017a,b). A large proportion of nitrate exists in coarse mode (PM_c, particle aerodynamic diameter > 2.5 μm) due to interactions with sea salt and mineral dust. The formation of nitrate on dust aerosols has been clearly observed using scanning electron microscopy (SEM), both in laboratory experiments and using field measurements (Li and Shao, 2009). Acid uptake of pollutants over sea salt and dust surfaces is important when evaluating coarse NO_3^-, as it modifies the chemical lifetime of nitric acid (including atmospheric loading and deposition). Continuous measurement of both fine- and coarse-mode aerosol compositions (including NO_3^-) is critical for achieving a complete understanding of the fate of air pollutants and changes in the Asian atmospheric environment (Li *et al*, 2012, Pan *et al*., 2017, Wang *et al*., 2017a).

Ground-based and airborne aerosol observations have been studied to determine the physics and chemistry of high-concentration events (e.g., Huebert *et al*., 2003; Jacob *et al.,* 2003, KORUS-AQ, 2016), but the duration of these observational campaigns is typically less than 1 month, which is insufficient for studying seasonal variation. Monitoring projects conducted by the Acid Deposition Monitoring Network in East Asia (EANET; 2014) and Asian Dust and Aerosol Lidar Observation Network (AD-Net Lidar; Sugimoto *et al*., 2008), among others, have been accumulating observational data for over 10 years, but detailed data on hourly aerosol compositions are rarely captured. Because seasonal changes in Asian monsoons play an important role in the patterns and frequency of long-range pollutant transport; therefore, long-term aerosol observations (over at least 1 year), including of aerosol composition and with a high time resolution, are required, but no such detailed observational studies have been undertaken to date.

We have made long-term synergetic observations of the behaviors of aerosols around the Chikushi Campus of Kyushu University, located in the suburbs of Fukuoka City (33.52°N, 130.47°E), since October 2013 (Pan *et al*., 2015, 2106; Itahashi *et al*., 2017; Uno *et al*., 2017a,b; Osada *et al*., 2016). We used a state-of-the-art aerosol observation instrument to measure

both fine- and coarse-mode aerosols. In this study, we report seasonal variation in both fine- and coarse-mode atmospheric aerosols based on long-term synergetic aerosol observations made at 1 h intervals in Fukuoka, Japan, from August 2014 to October 2015. During this period, several yellow sand and heavy pollutant transport episodes were observed. This paper reports on the major characteristics of anthropogenic aerosols and long-range dust transport, based on observations and chemical transport model (CTM) analysis. We also examined seasonal variations in fine- and coarse-mode long-range nitrate transport.

This report is structured as follows: Section 2 documents the observational dataset, Section 3 describes the CTM simulation in detail, Section 4 discusses temporal variations at observation sites and the model results, and Section 5 provides a summary and conclusions.

2 Observation

2.1 Aerosol Chemical Speciation Analyzer and NHx

A continuous dichotomous Aerosol Chemical Speciation Analyzer (ACSA-12 Monitor; Kimoto Electric Co., Ltd., Osaka, Japan), was utilized to measure PM_{10} (particulate matter < 10 μm in diameter) and $PM_{2.5}$ (particulate matter < 2.5 μm in diameter) with high temporal resolution (Kimoto *et al*., 2013). Particulate matter (PM) was collected on a tape filter made of Teflon (PTFE). Hourly observations were conducted to monitor SO_4^{2-}, NO_3^-, optical black carbon, and water-soluble organic compounds (WSOC) at Fukuoka. The mass concentrations of PM were determined using the beta-ray absorption method. The ACSA-12 measured NO_3^- and WSOC by an ultraviolet absorption-photometric method, and SO_4^{2-} by turbidimetry, after addition of $BaCl_2$ to form $BaSO_4$ and polyvinyl pyrrolidone as a stabilizer. The analytical period was within 2 h of sampling; therefore, the volatilization of particulate NH_4NO_3 after collection was regarded as minimal compared with the traditional filter-pack observation method. ACSA has been tested previously (Osada et al., 2016) and used to identify aerosol chemical compositions at Fukuoka (Pan *et al*., 2016, Uno *et al*., 2017a, 2017b). It should be noted that ACSA-12 measures both fine- and coarse-mode aerosols simultaneously and is an important for mass budget studies and evaluation of CTMs.

The behaviors of NH_3 and NH_4^+ are also important because they are the counter-ions for SO_4^{2-} and NO_3^-. Concentrations of gaseous NH_3 and NH_4^+ in fine particles were measured with a semi-continuous microflow analytical system (Kimoto Electric Co. Ltd., MF-NH_3A, Osada *et al.*, 2011). Two inlet lines were used to differentiate the total amounts of NHx and particulate NH_4^+ after gaseous NH_3 was removed using a phosphoric acid-coated denuder from the sample air stream. The cut-off diameter of the inlet impactor was about 2 μm (which is smaller than the ACSA $PM_{2.5}$ cut-off). Secondary inorganic aerosols (SO_4^{2-}, NO_3^-, and NH_4^+; SNA) were fully observed using our synergetic monitoring system.

Atmos. Chem. Phys. Discuss., https://doi.org/10.5194/acp-2017-447
Manuscript under review for journal Atmos. Chem. Phys.
Discussion started: 5 July 2017

Atmospheric Chemistry and Physics Discussions

2.2 Denuder-filter pack method

During our observation period from August 2014 to October 2015, we conducted denuder-filter (D-F) pack measurements at Fukuoka. An annular denuder–multi-stage filter sampling system was used for HNO_3 and size-segregated aerosol sampling. The sampling interval was 6−8 h for intensive observation and 1−2 days for regular observation. At the inlet, coarse-mode aerosols were removed by Nucleopore membrane filters (111114; Nomura Micro Science Co., Ltd., Atsugi, Japan [pore size = 8 μm]), and then gas-phase HNO_3 was collected with the annular denuder (2000-30x242-3CSS; URG Co., Chapel Hill, NC, USA) coated with NaCl (Perrino *et al*., 1990). Fine-mode aerosols were collected with a PTFE filter (J100A047A; ADVANTEC, Tokyo, Japan [pore size = 1 μm]), and a nylon filter (66509; Pall Co., Port Washington, NY, USA) captured volatized nitrates from the PTFE filter (Appel *et al*., 1981; Vecchi *et al.*, 2009). The sample air flow rate was 16.7 L min^{-1} (1 atm, 25°C). Under these conditions, the aerodynamic diameter of the 50% cut-off for the Nuclepore filter was approximately 1.9 μm (John *et al*., 1983). The samples were analyzed by ion chromatography (IC). Fine-mode aerosols (< 1.9 μm in diameter) were underestimated by the D-F pack compared with ACSA measurement, and coarse-mode aerosols (> 1.9 μm, with no upper limit) were overestimated by the D-F pack compared with the ACSA PM_c measurements (2.5−10 μm) due to the a difference in cut-off diameter between the methods (Osada et al., 2016). Details of the ACSA data comparison and validation were reported previously by Osada *et al*. (2016).

3 Numerical modeling

We used the 3-D Goddard Earth Observing System chemical transport model (GEOS-Chem) (ver. 09-02) (Bey *et al*., 2001, Park *et al.*, 2004, Fairlie *et al*., 2007, 2010). The model was run with the full GEOS-Chem NOx-Ox-VOC-HOx-CO chemistry option to simulate the formation of aerosols, including mineral dust, sea salt, and secondary inorganic aerosols. We also modeled the emission/transport of primary black carbon (BC) and organic carbon (OC). However, detailed carbonaceous species and secondary organic aerosols (SOA) options in GEOS-Chem were not used in this study.

Dust in GEOS-Chem is classified according to four size bins (radii of 0.1−1.0, 1.0−1.8, 1.8−3.0, and 3.0−6.0 μm), based on Ginoux *et al.* (2004). The smallest size bin is further divided into 4 bins (radii 0.1−0.18, 0.18−0.3, 0.3−0.6, 0.6−1.0 μm) for optical properties and heterogeneous chemistry. This model uses the dust entrainment and deposition (DEAD) mobilization scheme from Zender *et al*. (2003), combined with the source function used in the Goddard Chemistry Aerosol Radiation and Transport (GOCART) model (Ginoux *et al*. 2001), as described by Fairlie *et al*. (2007). Several modifications to capture seasonal changes in dust source function, the dust emission fraction within dust bins, and the change in wet scavenging efficiency that was inversely determined to fully capture Asian dust (Yumimoto *et al*., 2017) were used in this study. The general performance of our dust simulation was already reported by Yumimoto *et al*. (2017) and Uno *et al*. (2017a, b). Sea salt is distributed into two size bins (dry radii 0.01−0.5 and 0.5−8 μm). The sea salt emission scheme is based on the work of Jaeglé *et al*. (2011) and was well-validated by those authors. It includes the effects of sea-surface temperature (SST), as more sea salt is emitted in the summer.

Atmos. Chem. Phys. Discuss., https://doi.org/10.5194/acp-2017-447
Manuscript under review for journal Atmos. Chem. Phys.
Discussion started: 5 July 2017

Atmospheric Chemistry and Physics Discussions

In this study, the reactive uptake of HNO_3 and SO_2 on dust (limited by dust alkalinity), and the uptake of gas-phase H_2SO_4 (limited by competition with other aerosol surfaces) (Fairlie *et al*., 2010) were used. Dust-nitrate (mainly $Ca(NO_3)_2$) was simulated based on the heterogeneous reaction between dust and nitric acid, as follows:

$$CaCO_3 + 2HNO_3 \rightarrow Ca(NO_3)_2 + H_2O + CO_2 \quad (R1)$$

As described by Fairlie *et al*. (2010), the first-order reactive uptake rate constant (k) is calculated according to the uptake coefficient (γ) and surface area density of dust particles (A) using the following equation, suggested by Jacob (2000):

$$-\frac{dC}{dt} = \left[\frac{r}{D_g} + \frac{4}{c\,\gamma}\right]^{-1} A\,C = k\,C \qquad (1)$$

where C is the concentration of gas uptake (e.g., HNO_3), r is the aerosol particle radius, D_g is the molecular diffusion coefficient, and c is the mean molecular speed. The uptake coefficient depends on the ambient relative humidity (RH), and we used the RH-dependent function in Fig. 1 of Fairlie *et al*. (2010). More details on dust-nitrate formation from a heterogeneous reaction can be found in Fairlie *et al*. (2010). A similar heterogeneous reaction to that described by Eq. (1) for sea salt was also included in our calculation.

The model used the assimilated meteorological fields from the GEOS of the NASA Global Modeling and Assimilation Office (GMAO). The model has a horizontal resolution of 2° × 2.5° for global runs, and 0.5° × 0.667° for Asian one-way nesting runs (11°S−55°N, 70−150°E,), both having 47 vertical levels from the surface to 0.01 hPa. The lowest model layer thickness was approximately 130 m. We used anthropogenic emissions data from the Emission Database for Global Atmospheric Research (EDGAR) (Olivier and Berdowski, 2001) for the global domain and the Regional Emission Inventory in Asia (REAS) (ver. 2.1) for the Asian domain, as reported by Kurokawa *et al*. (2013). The REAS NH_3 emissions were modified to include seasonal variations in Asia based on Huang *et al*. (2012), and further changes in winter emissions recommended by Xu *et al* (2015). The model simulation was conducted from the beginning of December 2013 to the end of October 2015, and results from the first 8 months were used to train the model. Other basic numerical settings were as reported in Uno *et al.* (2017a, b).

To investigate whether domestic or transboundary air pollution is dominant in Japan, we also performed a sensitivity simulation. Because the quantity of emissions from China was larger than that from Japan, to avoid large nonlinearities in the atmospheric concentration response to emissions variation (e.g., Itahashi *et al*., 2015), a sensitivity simulation was designed to include a 20% reduction in anthropogenic emissions from Japan (defined as JOFF20%). Based on differences between the baseline simulation (CNTL) and the JOFF20% simulation, the domestic contribution from Japan (JOFF) was estimated using a multiple of 5 for differences in CNTL and JOFF20% experiments. We also made a volcanic SO_2 sensitivity simulation without volcanic SO_2 emissions (VOFF) because the SO_2 to SO_4^{2-} formation can be assumed to be linear.

Based on the analysis of PM concentrations, $PM_{2.5}$ and PM_{10} were calculated by summing the individual aerosol (SO_4^{2-}, NO_3^-, NH_4^+, BC and OC), dust, and sea salt components of the model. Hereafter, we denote modeled "ammonium" nitrate (i.e., NH_4NO_3) as A-NO_3^-, dust-nitrate as D-NO_3^-, sea salt nitrate as SS-NO_3^-, and their sum as simply NO_3^- (= A- + D- + SS-NO_3^-).

4 Results and Discussion

4.1 Meteorological variation and sea salt

Fig. 1 shows the location of the observation sites, Fukuoka and Mt. Sakurajima volcano, and the anthropogenic SO_2 emission distribution used in the model calculation. Fig. 2 shows (a) the daily mean and maximum wind speed, (b) the daily mean temperature, RH, and precipitation in Fukuoka, as observed by the Japan Meteorological Agency, and (c) the observed coarse-mode Na^+ by D-F, and GEOS-Chem-simulated coarse-mode sea salt (converted to Na^+ concentration).

Japanese weather is controlled by changes in Asian monsoons. Under summer monsoon conditions (covered by S-SE wind from the hot and moist air mass of the Pacific High), air temperature and RH are at their maximum, while during the winter monsoon (N-NW continental cold air outflow), low temperatures and less precipitation are observed in Fukuoka. Maximum wind speeds in excess of 10 m s^{-1} in summer−fall show the effects of typhoons (Fig. 2a). The precipitation difference between August 2014 and August 2015 is important for examining differences in the NH_3 concentration (August 2014 had more rainfall than August 2015).

The time variation of modeled coarse-mode Na^+ generally agreed well with observations, except during typhoon events. There were five typhoons between July and September 2015, and the modeled cNa^+ was very high compared with observations. This indicated that the sea salt emission scheme for very strong wind conditions was overestimated. We also observed high precipitation during the typhoon events. Another important difference is that the typhoon in 2014 occurred in the fall (September−October), after the SST had cooled, while in 2015 it occurred in the summer (July−August) when the SST was warm and more sea salt was emitted.

4.2 Time-series variations in $PM_{2.5}$, PM_{10}, black carbon, and CO

Fig. 3 (a)–(d) show the time variations (1h) in $PM_{2.5}$, $PM_{10,}$ optical BC (ACSA-12) and CO observations (Thermo Model 48) at Fukuoka. The figures also include the corresponding model values (2 h).

The observed $PM_{2.5}$ clearly exhibited frequent intermittent peaks from winter to early spring, but the frequency decreased after April according to the frequency of "polluted" cold air outbreaks from the Asian continent. The modeled $PM_{2.5}$ reproduced most of the observed variation. The modeled $PM_{2.5}$ value corresponded to approximately 58% of the observed $PM_{2.5}$ ($PM_{2.5\_model}$ = 0.58 ($PM_{2.5\_obs}$) + 1.16 µg m^{-3}, R = 0.72) because the observation data included aerosol compositions that were not incorporated into the model (e.g., secondary organic aerosols, many trace metals, and others).

The observed PM_{10} included coarse aerosols (e.g., dust and sea salt), and peaks corresponded to major dust events. Symbols A–G are the major dust events that occurred during our observation period (Uno *et al.*, 2017b). The time variation of modeled PM_{10} was in good agreement with observations, but was consistently underestimated for the same reasons as for $PM_{2.5}$ (i.e., more coarse aerosols were included in the observed data than in the model) and showed some uncertainty for large dust concentrations (Uno *et al.*, 2017b).

Modeled BC corresponded to approximately 33% of the observed BC (BC_{model} = 0.33 (BC_{obs}) + 0.23 μg m^{-3}, R = 0.35). Modeled BC was systematically underestimated from July to December, but was at reasonable levels during the winter. One possible explanation is underestimation of Japanese BC emission intensity (e.g., Itahashi *et al.*, 2017).

Modeled CO concentrations reproduced seasonal variation very well (winter = high and summer = low), but the modeled concentration level was 43% of the observed level (CO_{model} = 0.43 (CO_{obs}) + 21.2 ppb, R = 0.69). This may be due to underestimation of globally assumed background levels of CO. Observed CO and BC were highly correlated (R = 0.61), and a high CO concentration can be considered a product of long-range transport (LRT). From these comparisons of PM, BC, and CO, we found that the model simulation captured the major LRT outflow well, and can be used for detailed analysis of aerosol transport.

4.3 Daily and monthly variation in PM and aerosol compositions

Fig. 4 shows the daily average aerosol composition for (a) fine SO_4^{2-}, (b) fine NO_3^-, and (c) coarse NO_3^-. ACSA observations are indicated in blue; D-F pack observations are indicated by the red line (spike-like high peaks during the dust event are due to large particles [>10 μm, which is the cut-off in ACSA sampling]), and the gray shading indicates the model control experiment (CNTL). Yellow shading in Fig. 4(c) indicates the modeled dust-coarse NO_3^- (D-cNO_3^-) fraction. The modeled cNO_3^- is the sum of dust-nitrates and sea salt-nitrates.

Fig. 5 shows the monthly average (a) $PM_{2.5}$, (b) fine- and coarse-mode SO_4^{2-}, (c) fine and coarse NH_4^+, and (d) NH_3 gas. Box-whisker plots show the observed fine aerosol levels (10^{th}, 25^{th}, 50^{th}, 75^{th} and 90^{th} percentile values are marked). The observed average monthly coarse-mode aerosols are shown by the red dashed line. The modeled average monthly fine aerosol concentration for the CNTL is depicted by the straight black line, and by the black dashed line for the JOFF.

Fig. 6 shows the (a) HNO_3, (b) total NO_3^-, (c) coarse NO_3^-, and (d) fine NO_3^- levels. Observed values are shown in box-whisker plots. Modeled monthly averages are also shown. The JOFF model sensitivity experiment is denoted by the black dashed line in Fig. 6a, 6b, and 6d.

4.3.1 Fine-mode SO_4^{2-} and NH_4^+

The modeled SO_4^{2-} results explained the observed time variations and corresponded to 37% of the modeled $PM_{2.5}$ concentration ($SO_4^{2-}{}_{model}$ = 0.82($SO_4^{2-}{}_{obs}$) + 0.76 μg m^{-3}, R = 0.68; $SO_4^{2-}{}_{model}$ = 0.37($PM_{2.5\_model}$) + 0.40 μg m^{-3}, R = 0.81). The high correlation suggests that the variations in $PM_{2.5}$ were mainly driven by fSO_4^{2-}, as a main component of $PM_{2.5}$ for both the observations and the model.

Fig. 4a shows intermittent high SO_4^{2-} concentrations. High SO_4^{2-} levels in the winter depended on the frequency of LRT from the Asian continent, but high SO_4^{2-} levels are usually observed in summer (see also **Fig. 5b**). This is related to the meteorological conditions, i.e., high RH in summer. Fig. 4a shows high SO_4^{2-} levels from the end of July to early August 2015 (designated SF1 in the figure). These high SO_4^{2-} concentrations were due to Japanese domestic emissions and volcanic SO_2 emissions (see the appendix for a more detailed analysis).

The model underestimated SO_4^{2-} levels from December to January. Similar underestimation was observed in other CTM applications (Wang *et al.,* 2017b; Itahashi *et al*., 2017), and in the observations of He *et al.* (2014).

Based on Fig. 5, SO_4^{2-} and NH_4^+ levels are reasonably well predicted by the model. The JOFF sensitivity analysis showed that the contribution from Japanese emissions was small and the majority of SO_4^{2-} came from LRT from outside of Japan (annual mean Japanese domestic contribution = 15%). For NH_4^+, we found that the LRT contribution was large until April, after which the Japanese contribution increased as NH_3 emissions increased (annual mean Japanese domestic contribution = 27%).

Coarse mode SO_4^{2-} was about 0.1−0.2 of fine SO_4^{2-} (monthly average relationship: $cSO_4^{2-} = 0.185\ fSO_4^{2-} - 0.052$ μg m^{-3}, R = 0.66). The increases in coarse SO_4^{2-} contribution cannot be ignored in winter. Modeled cSO_4^{2-} levels were very small compared to observed levels and are not shown in the figure.

4.3.2 Fine-mode NO_3^-

The modeled fine NO_3^- reproduced the major time variations seen in the observed levels. NO_3^- levels are higher during the winter and lower during the summer, exhibiting clear seasonal changes. The winter (DJF) fNO_3^- average was 2.62 ± 1.64 μg m^{-3}. The daily maximum reached up to 6−9 μg m^{-3} and was sometimes higher than the SO_4^{2-} level, with the same timing of peaks as for SO_4^{2-}. This indicated that fNO_3^- were also controlled by LRT from the Asian continent (as discussed by Itahashi *et al*., 2017; Uno *et al*., 2017b). The JOFF sensitivity analysis also confirmed that the majority of fNO_3^- can be considered due to LRT from outside Japan during the winter. From mid-May−October, the Japanese contribution becomes dominant (annual mean Japanese domestic contribution = 53%).

In the summer, fNO_3^- is minimal because the NH_4NO_3 equilibrium between NH_3 and HNO_3 shifts to the gaseous phase under warm conditions. This phase shift is a function of temperature and RH, and it moves to an aerosol phase at cold temperatures. The monthly average fNO_3^- from June to September was 0.68 ± 0.34 μg m^{-3}. It should be noted that NO_3^- measurement by ACSA was finished within 2 h of PTFE sampling, so any artifact due to volatilization of NO_3^- from the Teflon filter surface was small (e.g., Osada *et al.*, 2016). As described in section 2, D-F measurement used the nylon backup file to catch the volatilized HNO_3 from the Teflon filter surface. Thus, both ACSA fNO_3^- and D-F fNO_3^- measurements showed consistent concentrations during the summer (average = 0.43−0.68 μg m^{-3}; see Fig. 4b.)

4.3.3 Coarse-mode NO_3^-

Fig. 4c shows that the coarse-mode NO_3^- had a distinct peak value during dust events A−G (D-F cNO_3^- levels are higher than ACSA cNO_3^- levels due to different upper cut-off limits). Modeled cNO_3^- levels were higher (see Fig. 4c and 6c) during the fall (October to November) and during the dust seasons (typically from February to June).

Fig. 6c shows the clear seasonal cycle of modeled cNO_3^-. The modeled results showed that dust-nitrate concentrations increased during dust episodes. Modeled sea salt-nitrate was consistently in the order of 0.5−1.0 μg m^{-3} as the baseline cNO_3^-, and it was the dominant except during the dust season (showing good agreement with observed values).

Table 1 summarizes the comparison of cNO_3^- levels. Except for January to June, sea salt-NO_3^- was the dominant within cNO_3^-, and the model results were in good agreement with actual observations. From January to June, the ratio of D-cNO_3^- to SS-cNO_3^- ≈ 1:1 and the modeled total cNO_3^- corresponded to two-thirds of the observed total cNO_3- (annual average ratio of D-cNO_3^- to SS-cNO_3^- ≈ 1 : 2.4). From January−June 2015, we observed several dust events (designated A−G). Uno *et al*. (2017b) described the typical onset of dust events B and C, and pointed out underestimation of the modeled cNO_3^- during these cold dust cases. In this paper, we examine dust event G as a case study of warm weather dust acid uptake validation.

Fig. 7 shows the daily changes in dust (colored region) and total D-cNO_3^- (contoured area) horizontal distributions from (a) June 12 to (b) June 13, and the Hybrid Single Particle Lagrangian Integrated Trajectory (HYSPLIT) model back trajectory starting from Fukuoka. It also shows a comparison of modeled and observed (c) fine- and (d) coarse-mode NO_3^-. The dust transport path was very similar to those of dust events B and C, as described by Uno *et al*. (2017b). For dust events B and C (see Fig. 4c), modeled cNO_3^- was underestimated, but for dust event G, modeled cNO_3^- levels were in good agreement with observed levels. Modeled results show that D-cNO_3^- mainly formed over the Yellow Sea and the East China Sea. This indicates that the underestimation of dust-NO_3^- over the winter was independent from the dust acid uptake scheme. These results indicate the importance of further studies on the mechanism of cNO_3^- formation.

4.3.4 Monthly variation in total NO_3 and NH_x

Fig. 8 shows the observed monthly variation in (a) NHx, (b) fNO_3^-, cNO_3^-, and HNO_3, and (c) the relative mass fraction of NO_3^- and HNO_3. From this figure, fNO_3^- clearly showed the highest concentration in winter, while HNO_3 increased in summer (HNO_3 accounted for 30−40% of total NO_3^-); this was due to the change in thermal equilibrium between gases and particles. Notably, cNO_3^- was always higher than fNO_3^- (cNO_3^- made up 27−55% of the total NO_3^-, and it exceeded 45% in winter). We observed 0.5−1.0 μg m^{-3} (0.2−0.4 ppb) of HNO_3 even in winter.

The observations showed that fine NH_4^+ is higher throughout the year, and NH_3 gas is also higher even in winter. This high NH_3 concentration may be influenced by local agriculture and poultry farming 5−10 km south of the observation site. The high NH_3 concentration (see Fig. 5d) in August 2015 (four times higher than August 2014) was due to differences in temperature and precipitation. The annual average cNH_4^+/total NH_x ratio was 10%, but it increased to 15% (JFM average). This indicates that the cNH_4^+ counterpart in winter is important for understanding cNO_3^- and cSO_4^{2-}.

Atmos. Chem. Phys. Discuss., https://doi.org/10.5194/acp-2017-447
Manuscript under review for journal Atmos. Chem. Phys.
Discussion started: 5 July 2017

Atmospheric Chemistry and Physics Discussions

The model results underestimated NH_3 and overestimated HNO_3; however, the modeled fNO_3^- and fNH_4^+ levels were in good agreement with the observed values (compared with Fig.4a,c,d). The NH_3 emissions inventory is at 25 km resolution, and does not include the impact of local agriculture and poultry farming (which has large uncertainty); this results in the decreased bias in NH_3 emissions seen in our study. However, this underestimation of NH_3 emissions was not a critical factor in the discussion of fNO_3^-, because the NH_4NO_3 equilibrium between NH_3 and HNO_3 is given as

$$HNO_{3\,(g)} + NH_{3\,(g)} \rightleftarrows NH_4NO_{3\,(p)} \quad (R2)$$

and the equilibrium constant is proportional to the product of partial pressure P_{NH3} and P_{HNO3}. The HNO_3-high (-low) and NH_3-low (-high) relationship may retain the same equilibrium constant, and this may be the reason for the agreement of fNH_4^+ and fNO_3^- levels with observed values. Most of the cNO_3^- formation occurred before arrival in Japan (it mainly occurred over the ocean), and was also not strongly sensitive to NH_3 emissions.

The present model does not include the formation scheme of cNH_4^+. The counterparts of cNH_4^+ can be cNO_3^- and cSO_4^{2-}, and this is one of the reasons for cNO_3^- underestimation by the model. It is important to describe the possible reasons for this underestimation to conduct a detailed N budget study, because the cNO_3^- fraction is very large. Another interesting question is whether the modeled acid-uptake scheme can explain the observed cNO_3^- levels in dust and sea salt. We used statistical analysis to investigate this.

4.4 Statistical analysis of coarse-mode NO_3^-

Major sources of cNO_3^- include dust, sea salt and other sources, represented as cNH_4^+. We conducted multiple regression analysis (MRA) to analyze cNO_3^-. We included cNa^+, nss-cCa^{2+} and cNH_4^+ as independent variables to describe the observed cNO_3^- (cSO_4^{2-} was excluded from the MRA due to its strong colinearity with cNH_4^+). One important point is that the observation site is surrounded by school grounds and a large city park, providing background local dust. We found that the median value of nss-cCa^{2+} during the non-dust season was 0.25 μg m^{-3}, and the residence time of local dust coming to the observation site for producing cNO_3^- was short (< 1 h). We excluded observations less than nss-cCa^{2+} < 0.25 μg m^{-3} from the MRA.

The result of the MRA (n = 160, nss-cCa > 0.25 μg m^{-3}) was

$$cNO_3^- = 0.51\ cNa^+ + 1.58\ \text{nss-}cCa^{2+} + 2.2\ cNH_4^+ + 0.19\ \mu g\ m^{-3}\ (R^2 = 0.74, p<0.001)$$

where the term on the right can be considered to represent SS-cNO_3^-, D-cNO_3^-, and cNO_3^- accompanied by cNH_4^+, respectively.

Fig. 9 shows the contribution of (a) MRA D-cNO_3^- = 1.58 × nss-cCa^{2+} for nss-cCa^{2+} > 0.25 μg m^{-3}, and (b) MRA SS-cNO_3^- = 0.51 × cNa^+. The figure also includes the GEOS-Chem modeled results (averaged over the same time period as for the D-F measurements). MRA D-cNO_3^- showed good agreement with modeled D-cNO_3^- levels (except for intensive dust events B and C), and this indicates that the dust acid-uptake scheme explains the observed dust-nitrate formation (underestimation for B and C comes from the underestimation of modeled dust concentrations). As previously pointed out, modeled SS-cNO_3^-

was overpredicted during the summer typhoon period; aside from these periods, good agreement was found with sea salt cNO_3 (Fig. 9b).

Fig. 10 shows the monthly averaged MRA results and clearly explains the observed seasonal variations. **Table 1** summarizes each term and shows the comparison with CTM. The average annual contribution of each term was 40% for SS-cNO_3^-, 20% for D-cNO_3^- and 40% for cNH_4^+ term. The D-cNO_3^- value was high during the dust season, and the sea salt component made the largest contribution throughout the year. The cNH_4^+ term made a large contribution during the winter, and one possible reason for this is the condensation/coagulation of small NH_4NO_3 and $(NH_4)_2SO_4$ particles onto large particles (e.g., sea salt and dust). The annual average D-cNO_3^- to SS-cNO_3^- ratio in MRA was 1 : 2, which is close to the modeled ratio (1 : 2.4), as shown in Table 1.

Our results suggest that inclusion of aerosol microphysical processes (such as condensation and coagulation of the fine anthropogenic aerosols NO_3^- and SO_4^{2-} onto the coarse particles) is important for exploring the observed cNO_3^- concentrations. A CTM incorporating advanced particle microphysics (APM) is one potential option (Yu and Luo, 2009). Such a modeling approach, incorporating interactions with mineral dust and sea salt, has not yet been fully explored in East Asia and is a future research direction.

5 Conclusions

Long-term synergetic fine- and coarse-mode aerosol observations were analyzed at 1 h intervals in Fukuoka, Japan, from August 2014 to October 2015. A GEOS-Chem chemical transport model including dust and sea salt acid uptake processes was used for detailed analysis of observation data to understand the effects of LRT from the Asian continent. The findings from this study can be summarized as follows:

1) Continuous measurement of SO_4^{2-}, NO_3^-, and optical BC with the ACSA-12 monitor, and of NH_4^+ and NH_3 with a semi-continuous microflow analytical system (MF-NH3A) in addition to D-F pack/IC analysis, established long-term synergetic fine- and coarse-mode aerosol data base in Fukuoka, Japan.
2) During the observation period, several Asian dust and long-range anthropogenic aerosol transport events were observed, and a numerical model generally explained the observed time variations. A dust concentration by dust emission inversion scheme effectively reproduced the major dust onset.
3) Numerical results explained the seasonal changes in fine aerosols (SO_4^{2-}, NO_3^-, and NH_4^+), and the impact of LRT, and a sensitivity analysis excluding Japanese domestic emissions revealed the LRT fraction (85% for fSO_4^{2-}, 47% for fNO_3^- and 73% for fNH_4^+).
4) Observational data for HNO_3, fNO_3^-, and cNO_3^- confirmed that there was a large amount of coarse NO_3^- comprising 40−55% of total nitrate during the winter; meanwhile, HNO_3 gas made up 40% of total nitrate in summer, and fine NO_3^-

peaked during the winter. A numerical model reproduced the seasonal variation in fine NO_3^-. For coarse NO_3^-, modeled cNO_3^- was in good agreement with observations between July and November (mainly coming from sea salt-NO_3^-).

5) Large-scale dust-nitrate outflow from China to Fukuoka was confirmed in all dust events. During the winter, modeled coarse NO_3^- was underestimated compared to the observed levels.

6) The coarse NO_3^- underestimation was examined statistically using multiple regression analysis (MRA). We included cNa^+, nss-cCa^{2+} and cNH_4^+ as independent variables to describe the observed cNO_3^-; these terms can be considered to represent SS-cNO_3^-, D-cNO_3^-, and cNO_3^- accompanied by cNH_4^+, respectively. The MRA results showed a high correlation, $R^2 = 0.74$, and clearly explained the observed seasonal changes. The annual average contributions of the component were 43% (SS-cNO_3^-), 19% (D-cNO_3^-), and 38% (cNH_4^+ term). The D-cNO_3^- component had the largest value during the dust season, and the sea salt component made a large contribution throughout the year. cNH_4^+ made a large contribution during the winter; one possible reason for this was the condensation/coagulation of small NH_4NO_3 and $(NH_4)_2SO_4$ particles onto large particles (e.g., dust and sea salt).

The present model did not include aerosol microphysical processes (such as condensation and coagulation between fine anthropogenic aerosols, such as NO_3^- and SO_4^{2-}, and coarse particles), but our results suggest that aerosol microphysical processes are important for studying observed cNO_3^- formation, especially in winter.

Data availability. To request observation data used in this study for scientific research purposes, please contact Itsushi Uno at Kyushu University via email (uno@riam.kyushu-u.ac.jp). Model simulations were based on GEOS Chem, open-source and publicly available software. The model and related software can be downloaded from http://acmg.seas.harvard.edu/geos/ for registered users.

Author contributions. Itsushi Uno designed the synergetic observations at Chikushi Campus of Kyushu University, Japan. Shigekazu Yamamoto and Kazuo Osada respectively carried out the ground-based ACSA and NHx-monitor observations at Fukuoka. Kazuo Osada conducted air sampling and chemical analysis for D-F pack samples during the observation period at Fukuoka. Yugo Kanaya and Xaiole Pan conducted the CO observations at Fukuoka. T. Duncan Fairlie provided GEOS Chem modeling system. Itsushi Uno, Keiya Yumimoto and Zhe Wang performed the model simulations and analysis, and prepared the paper with contributions from all coauthors.

Competing interests. The authors declare that they have no conflict of interest.

Acknowledgments. This work was supported by the Ministry of Education, Culture, Sports, Science and Technology (MEXT), the Japan Society for the Promotion of Science (JSPS) and the Grants-in-Aid for Scientific Research (KAKENHI)

program (Grant JP25220101). The authors would like to thank the developers of the GEOS reanalysis product. This work was partly funded by a collaborative research program through the Research Institute for Applied Mechanics at Kyushu University (no. 26AO-2, 27AO-6, 28AO-2). We thank Yusuke Kamiguchi at Nagoya University for D-F pack sampling and chemical analysis and Shohei Kuwahara at Kyushu University for D-F pack sampling.

5

References

Bey, I., J. Jacob, R. M. Yantosca, A. Logan, B. D. Field, A. M. Fiore, Q. Li, H. Y. Liu, J. Mickley, and M. G. Schultz: Global modeling of tropospheric chemistry with assimilated meteorology: Model description and evaluation, *J. Geophys. Res.*, **106**, 73–95, 2001.

EANET: EANET and Clean Air for Sustainable Development. The Third Report for Policy Makers (RPM3). Acid Deposition Monitoring Network in East Asia (EANET). Pathumthani, Thailand, 2014.

Fairlie, T.D., Jacob, D.J., Park, R.J.: The impact of transpacific transport of mineral dust in the United States, *Atmos. Environ.,* **41**, 1251–1266, 2007.

Fairlie, T.D., Jacob, D.J., Dibb, J.E., Alexander, B., Avery, M.A., A. van Donkelaar, Zhang, L.: Impact of mineral dust on nitrate, sulfate, and ozone in transpacific Asian pollution plumes, *Atmos. Chem. Phys.*, **10**, 3999–4012, 2010.

Genfa, Z., Dasgupta, P.K., Dong, S.: Measurement of atmospheric ammonia. *Environ. Sci. Technol.*, **23**, 1467–1474, 1989.

Ginoux, P., Chin, M., Tegen, I., et al.: Sources and distributions of dust aerosols simulated with the GOCART model, *J. Geophys. Res*., **106**(D17), 20255–20274, 2001.

Ginoux, P., Prospero, J. M., Torres, O., and Chin, M.: Long-term simulation of global dust distribution with the GOCART model: correlation with North Atlantic Oscillation, Environ. *Modell. Softw.*, **19**, 113–128, 2004.

He, H., Wang, Y., Ma, Q., Ma, J., Chu, B., Ji, D., Tang, G., Liu C., Zhang, H., Ho, J.: Mineral dust and NOx promote the conversion of SO2 to sulfate in heavy pollution days, *Scientific Reports*, **4**, 4172, doi:10.1038/srep04172, 2014.

Huang, X., Song, Y., Li, M., Li, J., Cai, X., Zhu, T., Hu, M., Zhang, H.: A high-resolution ammonia emission inventory in China, *Global Biogeochem. Cycles,* **26**, GB1030, doi:10.1029/2011GB004161, 2012.

Huebert, B. J., T. Bates, P. B. Russell, G. Shi, Y. J. Kim, K. Kawamura, G. Carmichael, and T. Nakajima: An overview of ACE-Asia: Strategies for quantifying the relationships between Asian aerosols and their climatic impacts, *J. Geophys. Res.*, **108(**D23), 8633, doi:10.1029/2003JD003550, 2003.

Irie, H., Muto, T., Itahashi, S., Kurokwa, J. and Uno, I.: Turnaround of tropospheric nitrogen dioxide pollution trends in China, Japan, and South Korea, *SOLA*, **12**, 170−174, doi:10.2151/sola.2016-035, 2016.

Itahashi, S. H. Hayami, I. Uno, X.L. Pan, M. Uematsu: Importance of coarse-mode nitrate produced via sea salt as atmospheric input to east Asian oceans. *Geophysical Research Letters*, **43**, doi:10.1002/2016GL068722, 2016.

Itahashi, S., Uno, I., Osada, K., Kamiguchi, Y., Yamamoto, S., Tamura, K., Wang, Z., Kurosaki, Y., Kanaya, Y.: Nitrate transboundary heavy pollution over East Asia in winter, *Atmos. Chem. Phys.*, **17**, 3823-3843, 2017.

Jacob, D.: Heteogeneous chemistry and tropospheric ozone, *Atmos. Environ.*, **34**, 2131-2159, 2000.

Jacob, D., J. Crawford, M. Kleb, V. Conners, R. Bendura, J. Raper, G. Sachse, J. Gille, and L. Emmons: Transport and chemical evolution over the Pacific (TRACE-P) mission: Design, execution, and overview of first results, *J. Geophys. Res*., **108**(D20), 8781, doi:10.1029/2002JD003276, 2003.

Kimoto, H., Ueda, A., Tsujimoto, K., Mitani, Y., Toyasaki, Y. and Kimoto, T.: Development of continuous dichotomous aerosol chemical speciation analyzer, *Clean Technol.*, **23**, 49–52, 2013 (in Japanese).

KORUS-AQ: https://espo.nasa.gov/home/korus-aq/content/KORUS-AQ.

Kurokawa, J., Ohara, T., Morikawa, T., Hanayama, S., Janssens-Maenhout., G, Fukui, T., Kawashima, K., Akimoto, H.: Emissions of air pollutants and greenhouse gases over Asian regions during 2000–2008: Regional Emission inventory in ASia (REAS) version 2, *Atmos. Chem. Phys.*, **13**, 11019–11058, 2013.

Lawrence, M.G., Lelieveld, J.: Atmospheric pollutant outflow from southern Asia: a review. *Atmospheric Chemistry and Physics,* **10**, 11017-11096, 2010.

Li, J., Du, H., Wang, Z., Sun, Y., Yang, W., Li, J., Tang, X., Fu, P.: Rapid formation of a severe regional winter haze episode over a mega-city cluster on the North China Plain. *Environmental Pollution,* **223**, 605-615, 2017.

Li, W.J., Shao, L.Y.: Observation of nitrate coatings on atmospheric mineral dust particles. *Atmospheric Chemistry and Physics,* **9**, 1863-1871, 2009.

Li, J., Wang, Z.F., Zhuang, G., Luo, G., Sun, Y., Wang, Q.: Mixing of Asian mineral dust with anthropogenic pollutants over East Asia: a model case study of a super-duststorm in March 2010. *Atmospheric Chemistry and Physics,* **12**, 7591-7607, 2012.

Ohara, T., *et al*.: REAS: Asian emission inventory for anthropogenic emission sources during the period 1980– 2020, *Atmos. Chem. Phys*., **7**, 4419– 4444, 2007.

Oita, A., Malik, A., Kanemoto, K., Geschke, A., Nishijima, S., and Lenzen, M.: Substantial nitrogen pollution embedded in international trade. *Nat. Geosci.* **9**, 111–115, 2016.

Olivier, J.G.J. and J.J.M. Berdowski, *Global emissions sources and sinks*. In: Berdowski, J., Guicherit, R. and B.J. Heij (eds.) *The Climate System*, 33-78. A. A. Balkema Publishers/Swets & Zeitlinger Publishers, Lisse, The Netherlands, 2001.

Osada, K., Ueda, S., Egashira, T., Takami, A., Kaneyasu, N.: Measurement of gaseous NH3 and particulate NH4+ in the atmosphere by fluorescent detection after continuous air-water droplet sampling, *Aerosol and Air Quality Research,* **11**, 170–178, 2011.

Osada, K., T. Kamikuchi, S. Yamamoto, S. Kuwahara, X. Pan, Y. Hara, I. Uno: Comparison of ionic concentrations on size-segregated atmospheric aerosol particle based on a denuer-filter method and a Continuous Dichotomous Aerosol Chemical Speciation Analyzer (ACA-12), *Earozoru Kenkyu*, **31**, 203–209, 2016 (in Japanese with English abstract).

Pan, X., Uno, I., Wang, Z., Nishizawa, T., Sugimoto, N., Yamamoto, S., Kobayashi, H., Sun, Y., Fu, P., Tang, X., Wang, Z.: Real-time observational evidence of changing Asian dust morphology with the mixing of heavy anthropogenic pollution. *Scientific Reports* **7**, 335, DOI:10.1038/s41598-017-00444-w, 2017.

Pan, X., Uno, I., Hara, Y., Kuribayashi, M., Kobayashi, H., Sugimoto, N., Yamamoto, S., Shimohara, T., Wang, Z.: Observation of the simultaneous transport of Asian mineral dust aerosols with anthropogenic pollutants using a POPC during a long-lasting dust event in late spring 2014. *Geophysical Research Letters* **42**, 1593-1598, 2015.

Park, R. J., Jacob, D. J., Field, B. D., Yantosca, R. M., Chin, M.: Natural and transboundary pollution influences on sulphate-nitrate-ammonium aerosols in the United States: implications for policy, *J. Geophys. Res*., **109**, D15204, doi:10.1029/2003JD004473, 2000.

Richter, A., J. P. Burrows, H. Nüβ, C. Granier, and U. Niemeier: Increase in tropospheric nitrogen dioxide over China observed from space. *Nature*, **437**, 129−132, doi:10.1038/nature04092, 2005.

Uno, I., Yumimoto, K., Pan, X. L., Wang, Z., Osada, K., Itahashi, S., Yamamoto, S.: Simultaneous dust–pollutants transport over East Asia: the Tripartite Environment Ministers Meeting March 2014 Case Study, *SOLA,* **13**, 47-52, doi:10.2151/sola.2017-009, 2017a.

Uno, I., K. Osada, K. Yumimoto, Z. Wang, S. Itahashi, X. Pan, Y. Hara, S. Yamamoto and T. Nishizawa: Importance of long-range nitrate transport based on long-term observation and modeling of dust and pollutants over East Asia, *Aerosol and Air Quality Research,* **17***, doi:10.4209/aaqr.2016.11.0494,* 2017b.

Wang, Z., Pan, X., Uno, I., Li, J., Wang, Z., Chen, X., Fu, P., Yang, T., Kobayashi, H., Shimizu, A., Sugimoto, N., Yamamoto, S.: Significant impacts of heterogeneous reactions on the chemical composition and mixing state of dust particles: A case study during dust events over northern China, *Atmospheric Environment*, **159**, 83−91, 2017a.

Wang, Z., Pan, X., Uno, I., Li, J., Wang, Z., Sugimoto, N., Yamamoto, S.: Modeling the long-range transport of particulate matters during winter in East Asia using NAQPMS and CMAQ, *Aerosol and Air Quality Research*, **17,** doi: 10.4209/aaqr.2016.12.0534, 2017b.

Xu, P. *et al*.: An inventory of the emission of ammonia from agriculture fertilizer application in China for 2010 and its high-resolution spatial distribution, *Atmos. Environ*. **115**, 141–148, 2015.

Yu, F. and Luo, G.: Modeling of gaseous methylamines in the global atmosphere: impacts of oxidation and aerosol uptake, *Atmos. Chem. Phys*., **14**, 12455-12464, doi:10.5194/acp-14-12455-2014, 2014.

Yumimoto, K., I. Uno, X. Pan, T. Nishizawa, S.-W. Kim: Inverse Modeling of Asian Dust Emission with POPC Observations for TEMM DSS 2014 Case Study, *SOLA,* **13**, 31−35, doi:10.2151/sola.2017- 006, 2017.

Zender, C. S., Bian, H., and Newman, D.: Mineral Dust Entrainment And Deposition (DEAD) model: Description and 1990s dust climatology, *J. Geophys. Res*., **108**(D14), 4416, doi:10.1029/2002JD002775, 2003.

Zhang, Q., Jiang, X., Tong, D., J. Davis, S.J., Zhao, H., Geng, G., Feng, T., Zheng, B., Zifeng, L., Streets, D.G., Ni, R., Brauer, M., van Donkelaar, A., Martin, R.V., Huo, H., Liu, Z., Da Pan, D., Kan, H., Yan, Y., Lin, J., He, K., and Guan, D.: Transboundary health impacts of transported global air pollution and international trade, *Nature* **543**, 705–709, doi:10.1038/nature21712, 2017.

Atmos. Chem. Phys. Discuss., https://doi.org/10.5194/acp-2017-447
Manuscript under review for journal Atmos. Chem. Phys.
Discussion started: 5 July 2017

Atmospheric Chemistry and Physics Discussions

Appendix

During the SF1 period (shown in Fig. 4), two typhoons passed south of Japan from east to west. Fig. A1 shows snapshots of the trajectories and wind fields of Typhoon Halola (T12) and Typhoon Soudelor (T13), along with modeled SO_4^{2-} concentrations.

SO_4^{2-} in the northern part of Japan and Korea were under the control of long-range transport from China, while the southern part of Japan was covered by east winds (due to typhoons). This indicated that the high SO_4^{2-} concentrations in Fukuoka were due to Japanese domestic emissions and the impact of Mt. Sakurajima volcano (typically August 2−6). Note that the estimated SO_2 emission from Mt. Sakurajima is around 10^3 Gg $year^{-1}$, which is almost equivalent to the level of anthropogenic SO_2 emissions in Japan.

Fig. A2 shows the volcano sensitivity experiment (VOFF) for SO_4^2. It is clear that the impact of the volcano was higher for the period August 2−6; during this period, SO_4^{2-} contributions converted from volcanic SO_2 emission exceeded 50% of the total SO_4^{2-}. Observations show higher values from July 27−August 1, and the model simulation failed to describe this. Volcanic emissions are natural phenomena and have strong day-by-day variation, so this failure of the model is due to underestimation of volcanic emissions during this period.

Atmos. Chem. Phys. Discuss., https://doi.org/10.5194/acp-2017-447
Manuscript under review for journal Atmos. Chem. Phys.
Discussion started: 5 July 2017

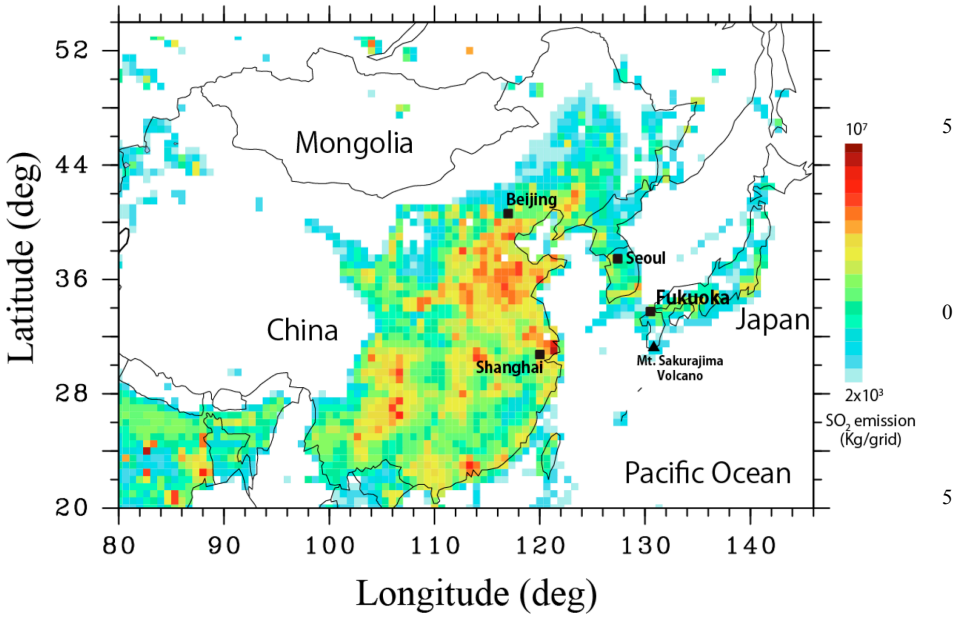

20

Figure 1. SO_2 emissions intensity (based on 2008 data) and observation sites: Fukuoka and Mt. Sakurajima volcano.

Atmos. Chem. Phys. Discuss., https://doi.org/10.5194/acp-2017-447
Manuscript under review for journal Atmos. Chem. Phys.
Discussion started: 5 July 2017

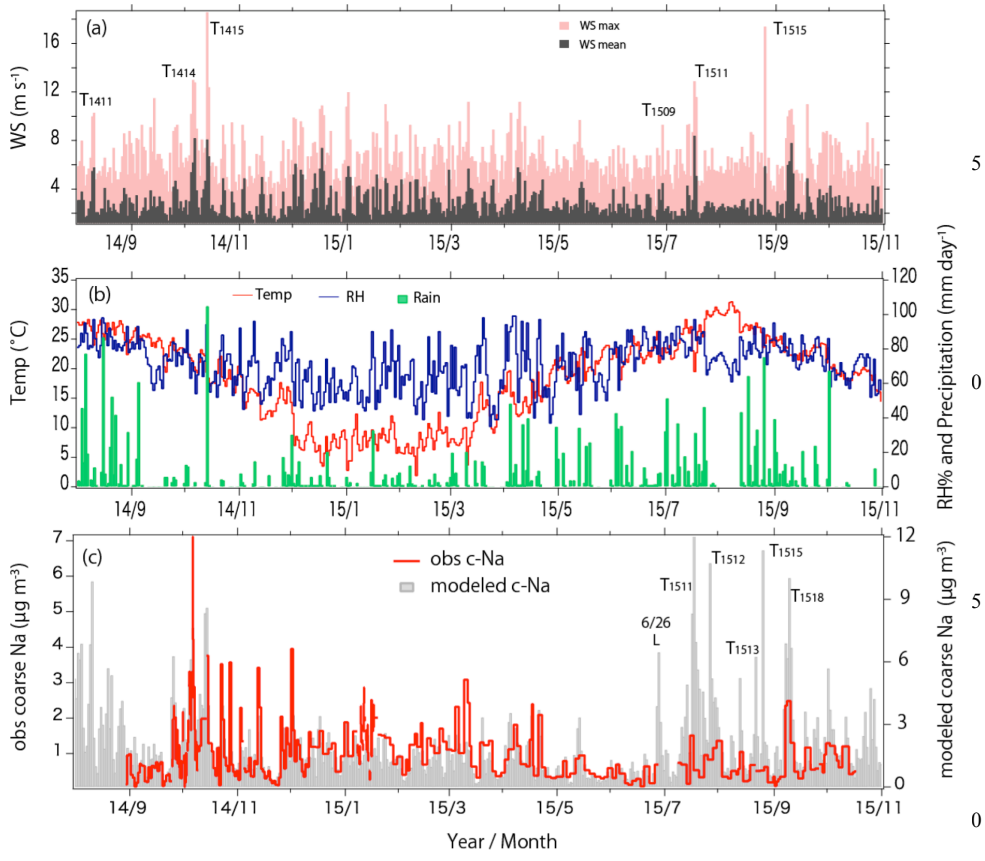

Figure 2. (a) Wind speeds (daily mean and maximum) at Fukuoka. (b) Daily average temperature, relative humidity (RH) and precipitation. (c) Observed coarse Na^+ and modeled coarse Na^+ (converted from GEOS-Chem coarse sea-salt (SALC)). Tyyxx indicates typhoons: T1411 = Halong, T1414 = Fengshen, T1415 = Kalmaegi, T1509 = Chanhom, T1511 = Nangka, T1512 = Halola, T1513 = Soudelor, T1515 = Goni, T1518 = Etau.

Atmos. Chem. Phys. Discuss., https://doi.org/10.5194/acp-2017-447
Manuscript under review for journal Atmos. Chem. Phys.
Discussion started: 5 July 2017

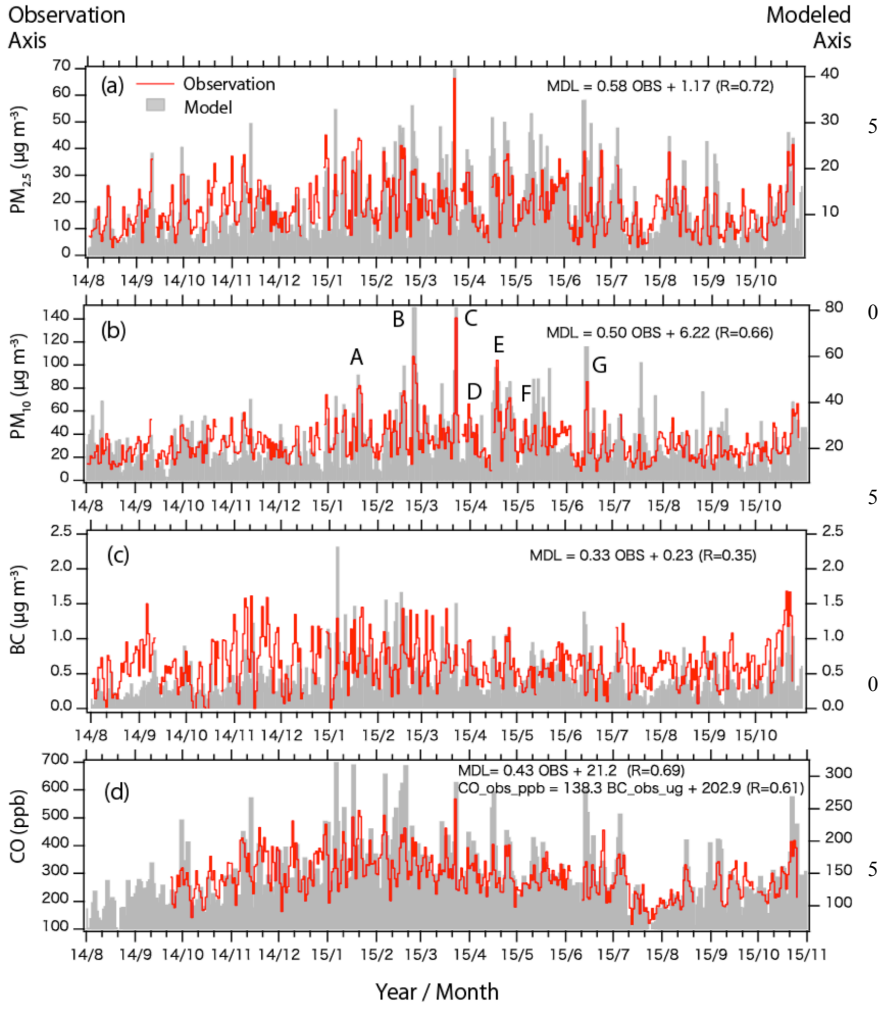

30 **Figure 3. Daily average (a) particulate matter < 2.5 μm diameter ($PM_{2.5}$), (b) particulate matter < 10 μm diameter (PM_{10}), (c) black carbon (BC), and (d) CO. Red lines show the observed values, and gray shading indicates the numerical results. Observed data are on the left axis and numerical results are on the right axis, scaled by the regression results (except for c). Symbols A–G in (b) indicate major dust events in Fukuoka.**

Atmos. Chem. Phys. Discuss., https://doi.org/10.5194/acp-2017-447
Manuscript under review for journal Atmos. Chem. Phys.
Discussion started: 5 July 2017

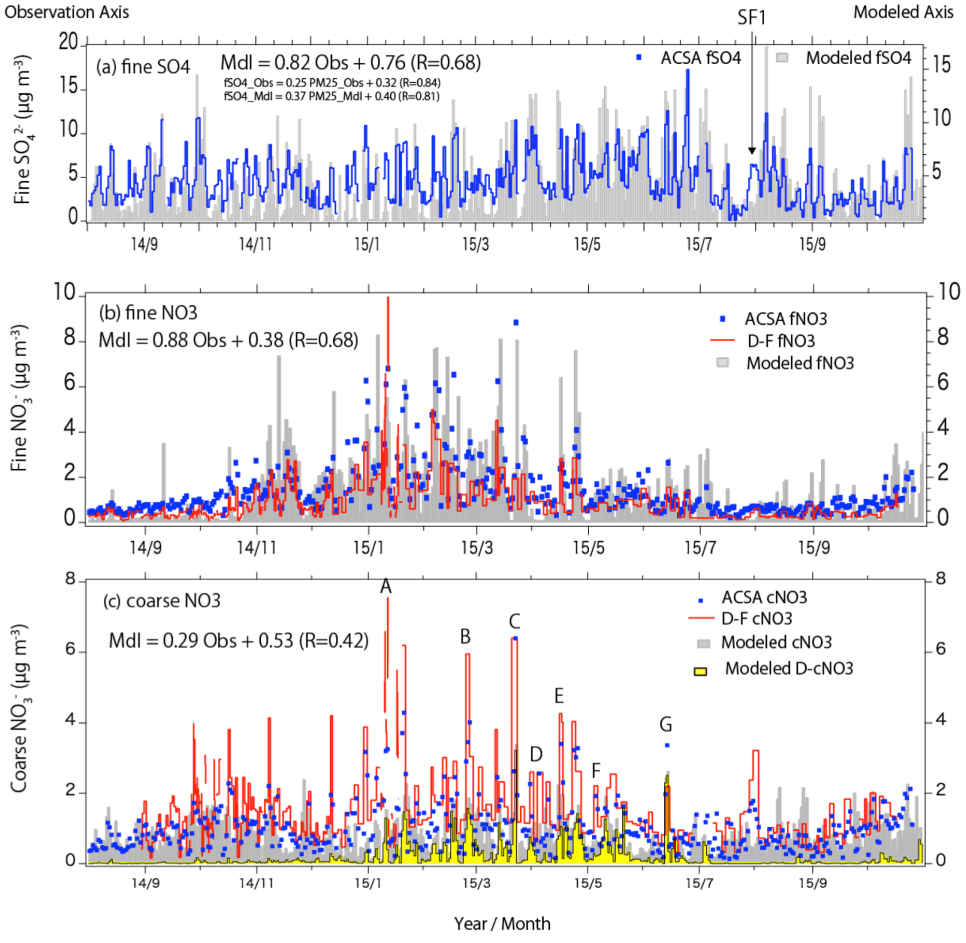

Figure 4. Daily average variation in (a) fine SO_4^{2-}, (b) fine NO_3^-, and (c) coarse NO_3^-. The blue line and dots show Aerosol Chemical Speciation Analyzer (ACSA) observations, the red line indicates measurements from the denuder filter pack (D-F) method, and gray shading indicates the model simulation. D-F data are sampling period averages.

Atmos. Chem. Phys. Discuss., https://doi.org/10.5194/acp-2017-447
Manuscript under review for journal Atmos. Chem. Phys.
Discussion started: 5 July 2017

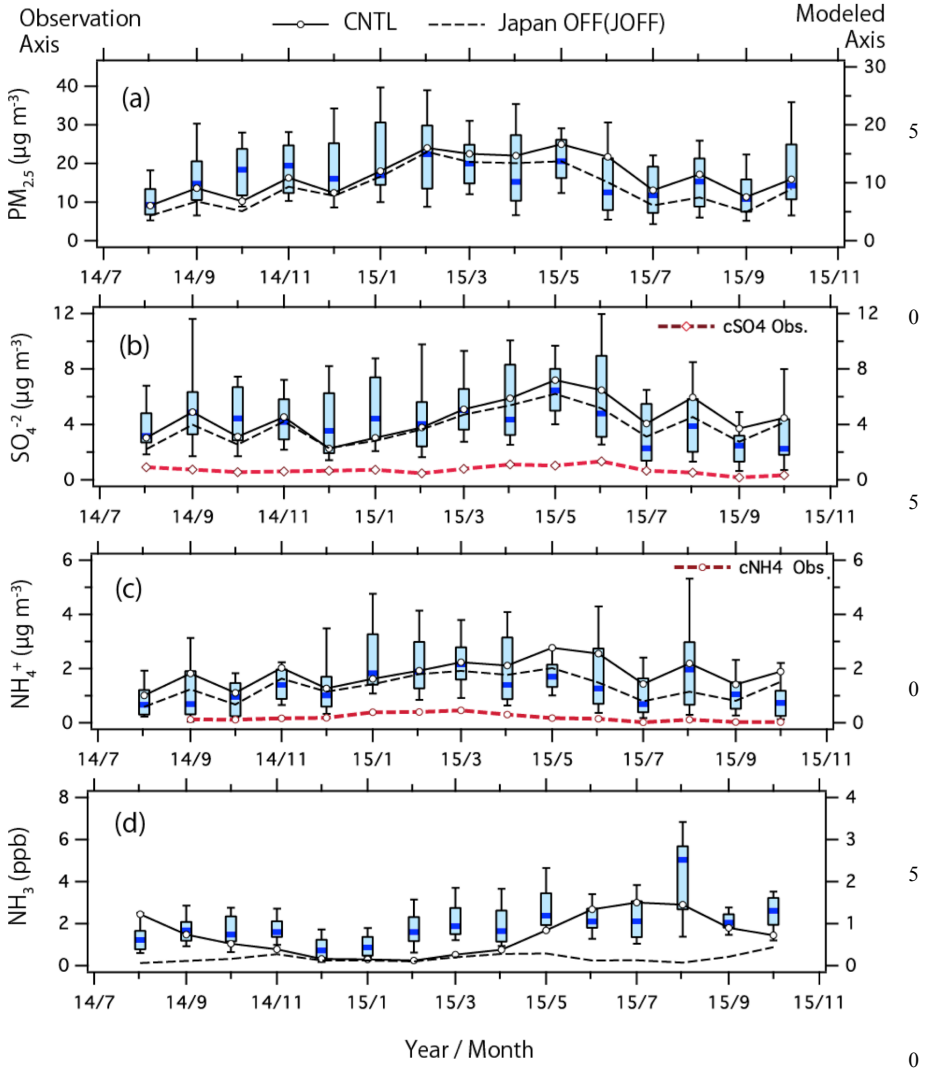

Figure 5. Monthly average plots of (a) $PM_{2.5}$, (b) fine SO_4^{2-}, (c) fine NH_4^+, and (d) NH_3 gas. Box-whisker plots show observations (10^{th}, 25^{th}, 50^{th}, 75^{th}, 90^{th} percentile values). Red lines in (b) and (c) show ACSA-observed coarse mode concentrations. Black lines are modeled monthly averages; the straight line indicates the baseline model (CNTL), and the dashed line indicates the domestic emissions contribution from Japan (JOFF).

Atmos. Chem. Phys. Discuss., https://doi.org/10.5194/acp-2017-447
Manuscript under review for journal Atmos. Chem. Phys.
Discussion started: 5 July 2017

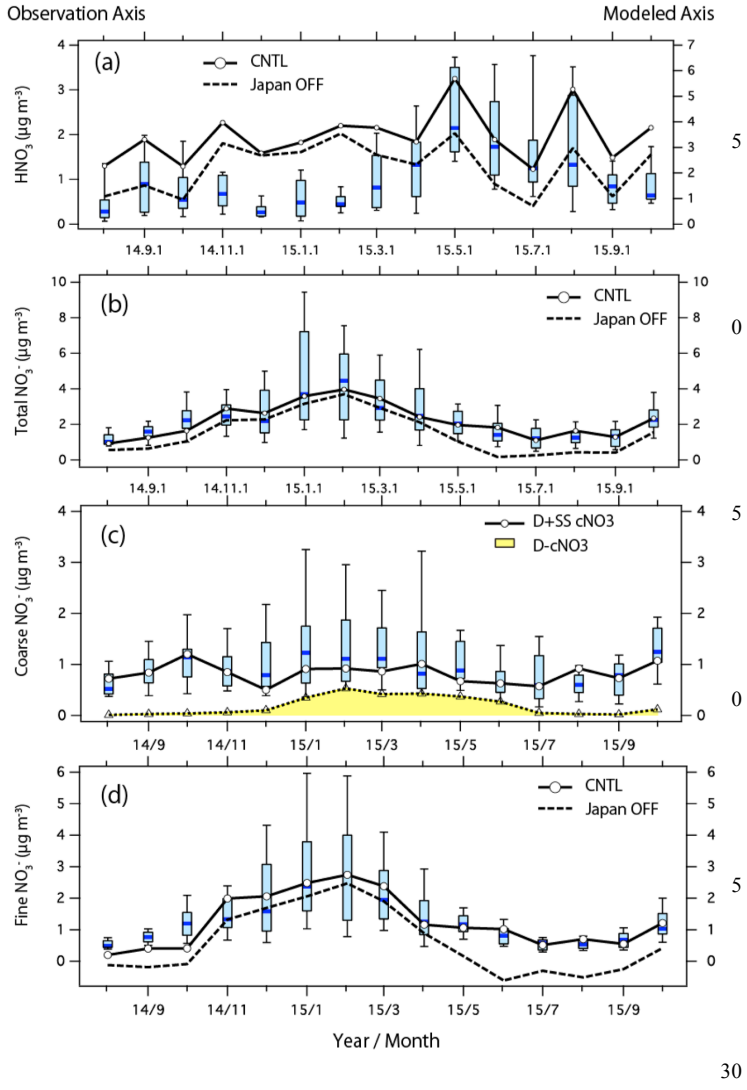

Figure 6. Monthly average (a) HNO_3, (b) total NO_3^-, (c) coarse NO_3^-, and (d) fine NO_3^-. Box-whisker plots show observations (10^{th}, 25^{th}, 50^{th}, 75^{th}, 90^{th} percentile values), and black lines are modeled monthly averages; the straight line indicates CNTL, and the dashed line, except in (c), indicates JOFF. For (c), the dashed line shows the modeled dust-coarse NO_3^- (D-cNO_3^-). HNO_3 observations are from D-F, and NO_3^- observations are from ACSA.

Atmos. Chem. Phys. Discuss., https://doi.org/10.5194/acp-2017-447
Manuscript under review for journal Atmos. Chem. Phys.
Discussion started: 5 July 2017

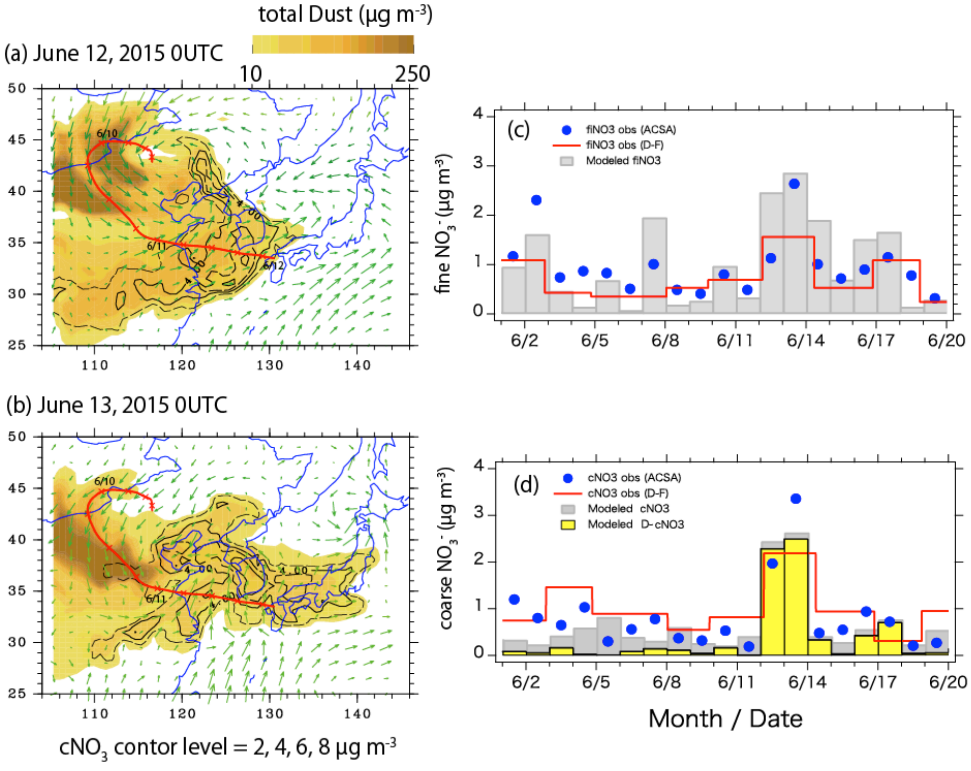

Figure 7. Horizontal distribution of dust (sum of all dust bins) (yellow color) and fine NO_3^- (contour) with wind vectors for (a) June 12, (b) June 13, and the time variation of daily average (c) fine NO_3^- and (d) coarse NO_3^-.

Atmos. Chem. Phys. Discuss., https://doi.org/10.5194/acp-2017-447
Manuscript under review for journal Atmos. Chem. Phys.
Discussion started: 5 July 2017

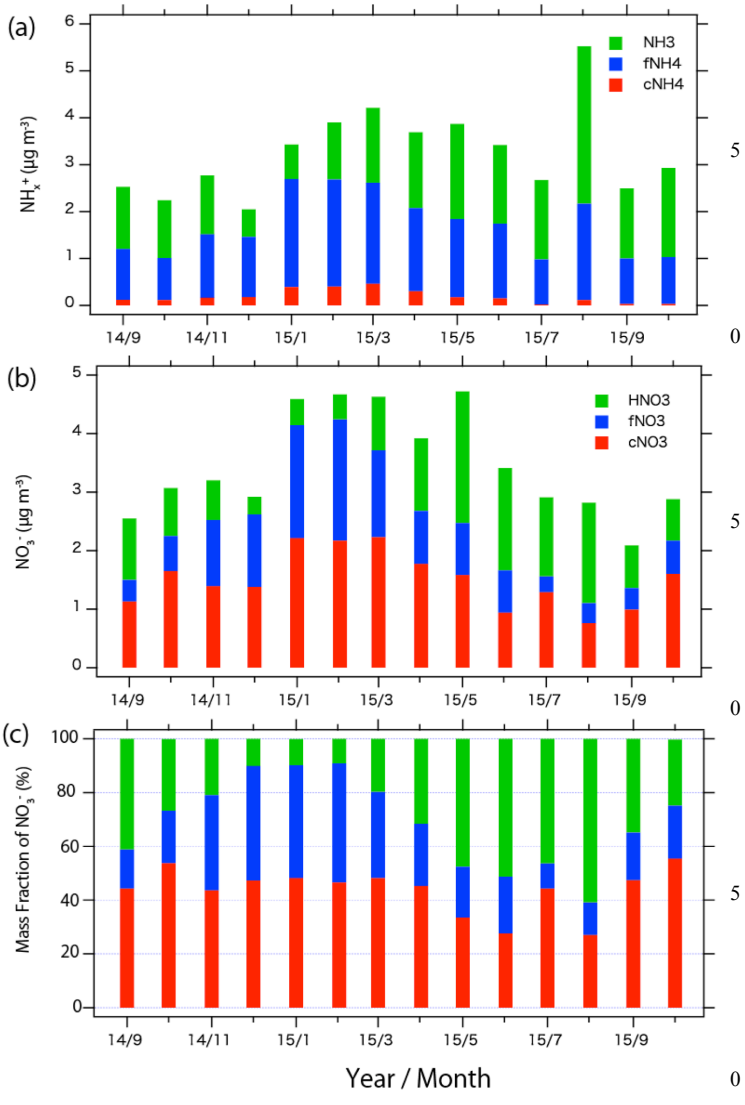

Figure 8. Monthly average values for (a) NHx, (b) NO_3, and (c) the mass fraction (%) of NO_3, observed by D-F.

Atmos. Chem. Phys. Discuss., https://doi.org/10.5194/acp-2017-447
Manuscript under review for journal Atmos. Chem. Phys.
Discussion started: 5 July 2017

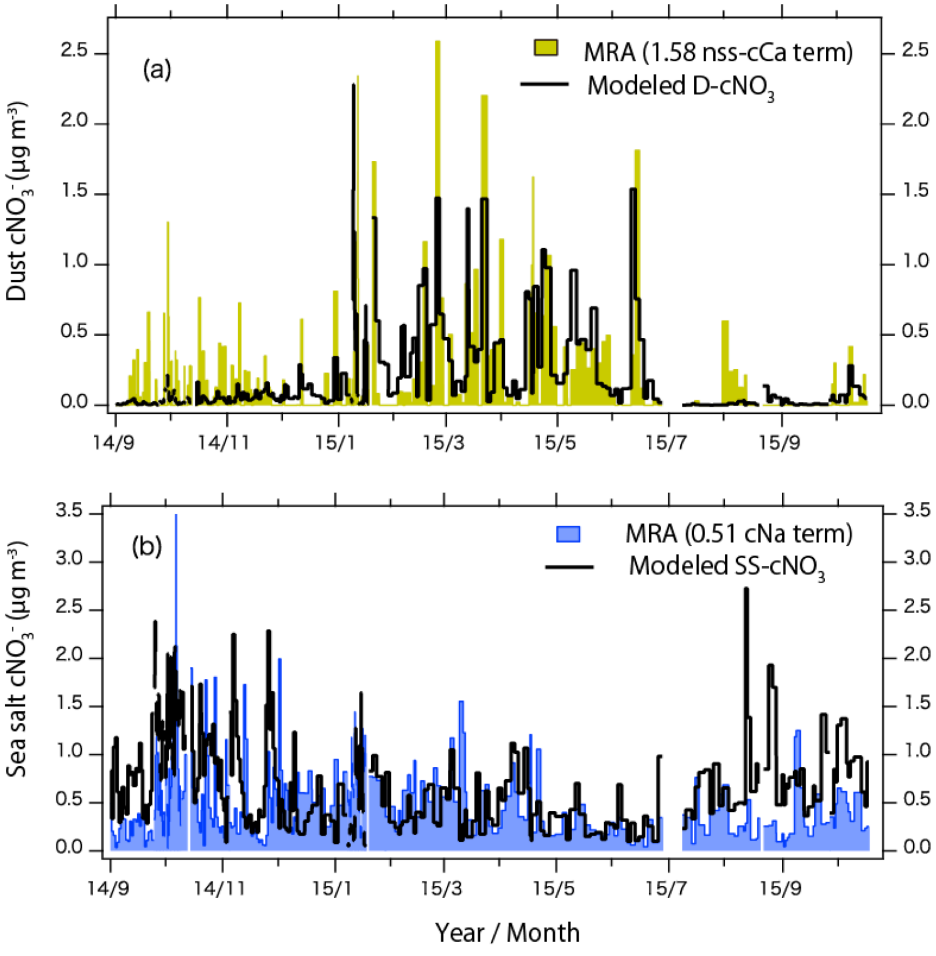

Figure 9. (a) D-cNO$_3^-$ estimated by multiple regression analysis and modeled D-cNO$_3^-$, (b) the same parameters for sea salt-NO$_3^-$. Modeled results averaged over the same time period as for the D-F measurements.

Atmos. Chem. Phys. Discuss., https://doi.org/10.5194/acp-2017-447
Manuscript under review for journal Atmos. Chem. Phys.
Discussion started: 5 July 2017

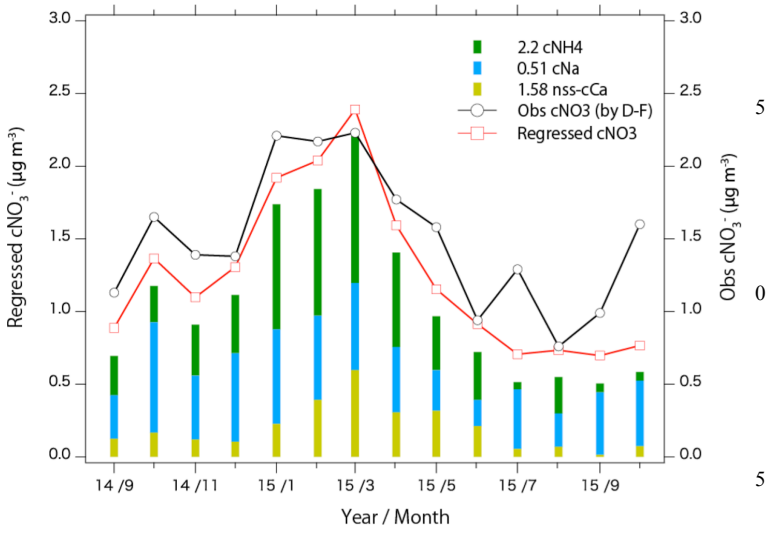

Figure 10. Monthly average multiple regression results for the dust-cNO_3^-, sea salt-cNO_3^-, and cNH_4^+-related components.

20

Atmos. Chem. Phys. Discuss., https://doi.org/10.5194/acp-2017-447
Manuscript under review for journal Atmos. Chem. Phys.
Discussion started: 5 July 2017

Atmospheric Chemistry and Physics Discussions

Appendix

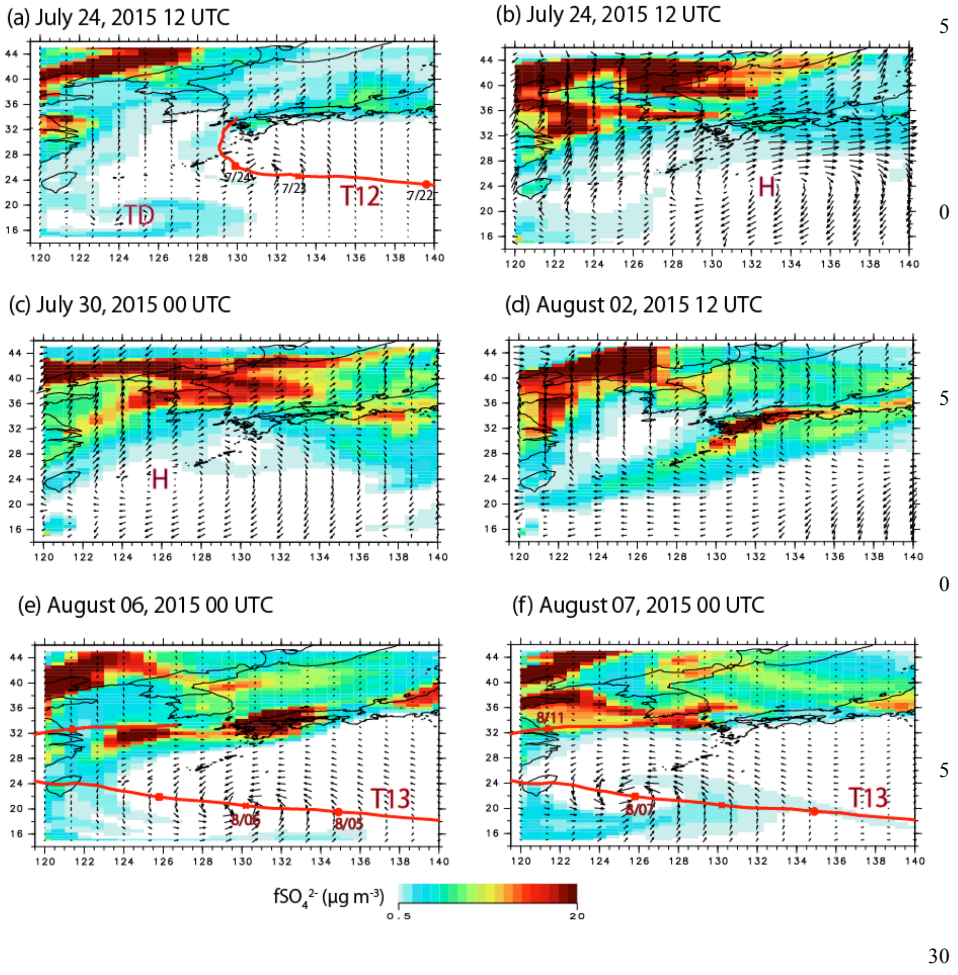

Figure A1. Horizontal distribution of fine SO_4^{2-} (color) with wind vectors from model's first vertical level (65 m). The red line indicates the trajectory of Typhoon Halola (T12) in (a), and Typhoon Soudelor (T13) in (e) and (f).

Atmos. Chem. Phys. Discuss., https://doi.org/10.5194/acp-2017-447
Manuscript under review for journal Atmos. Chem. Phys.
Discussion started: 5 July 2017

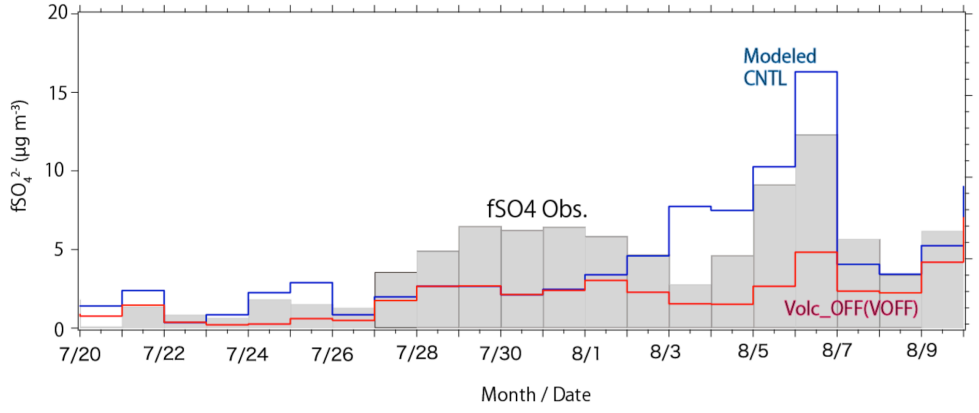

Figure A2. Daily average variation in observed (gray shading) and modeled fine SO_4^{2-} (blue line = CNTL and red line = VOFF).

Atmos. Chem. Phys. Discuss., https://doi.org/10.5194/acp-2017-447
Manuscript under review for journal Atmos. Chem. Phys.
Discussion started: 5 July 2017

Atmospheric Chemistry and Physics Discussions

Table 1. Comparison of coarse-mode NO_3^- levels (μg m^{-3})

Period	Observation	CTM			Mult. Regress. Analysis		
	cNO_3^-	D-cNO_3^-	SS-cNO_3^-	Total-cNO_3^-	D-cNO_3^-	SS-cNO_3^-	cNH_4
Jan.−June	1.29[a] (1.82)[b]	0.40	0.43	0.83	0.34	0.46	0.68
Sept.−Dec., July	0.94 (1.37)	0.06	0.73	0.79	0.11	0.50	0.26
Annual[c]	1.13 (1.61)	0.24	0.58	0.82	0.24	0.48	0.49

a ACSA observation.

b D-F observation.

c Average level between Sept. 2014 and July 2015 (excluding typhoon period).